# Vacancy-induced nanoscale phase separation in $K_xFe_{2-y}Se_2$ single crystals evidenced by Raman scattering and powder x-ray diffraction

N. Lazarević,[1] M. Abeykoon,[2] P. W. Stephens,[3,4] Hechang Lei (雷和畅),[2] E. S. Bozin,[2] C. Petrovic,[2] and Z. V. Popović[1]

[1]*Center for Solid State Physics and New Materials, Institute of Physics Belgrade, University of Belgrade, Pregrevica 118, 11080 Belgrade, Serbia*

[2]*Condensed Matter Physics and Materials Science Department, Brookhaven National Laboratory, Upton, New York 11973-5000, USA*

[3]*Department of Physics and Astronomy, State University of New York, Stony Brook, NY 11794-3800, USA*

[4]*Photon Sciences Directorate, Brookhaven National Laboratory, Upton, New York 11973-5000, USA*

(Received 7 May 2012; revised manuscript received 10 July 2012; published 6 August 2012)

Polarized Raman scattering spectra of $K_xFe_{2-y}Se_2$ were analyzed in terms of peculiarities of both $I4/m$ and $I4/mmm$ space group symmetries. The presence of the Raman active modes from both space group symmetries (16 Raman-active modes of the $I4/m$ phase and two Raman-active modes of the $I4/mmm$ phase) confirmed the existence of two crystallographic domains with different space group symmetry in a $K_xFe_{2-y}Se_2$ sample. High-resolution synchrotron powder x-ray diffraction structural refinement of the same sample confirmed the two-phase description, and determined the atomic positions and occupancies for both domains.

DOI: 10.1103/PhysRevB.86.054503 PACS number(s): 78.30.−j, 74.25.−q, 61.05.cp, 61.72.jd

The recent discovery of block checkerboard antiferromagnetic order of superconducting materials $A_xFe_{2-y}Se_2$ ($A = K$, Rb, Cs, and Tl) has invoked considerable debate in the scientific community.[1–6] It was shown that the appearance of antiferromagnetism is a consequence of the Fe vacancy ordering.[7,8] These unique properties among the superconductors opened a question whether Fe vacancies stabilize or destroy the superconductivity. Very recently, scanning tunneling microscopy (STM) measurements,[9] conducted on $K_xFe_{2-y}Se_2$ thin films grown by molecular beam epitaxy, revealed that the $K_xFe_{2-y}Se_2$ sample contains two distinct phases: an insulating phase with well defined $\sqrt{5} \times \sqrt{5}$ order of Fe vacancies, and a superconducting $KFe_2Se_2$ phase containing no Fe vacancies. It was found that the presence of a single Fe vacancy locally destroys superconductivity.[9] Recent Angle-resolved photoemission spectroscopy (ARPES) and optical measurements combined with TEM analysis[10,11] also show the presence of the nanoscale phase separation between superconducting and antiferomagnetic phases in bulk crystals.

Raman scattering (RS) measurements of $K_xFe_{2-y}Se_2$ were analyzed, to the best of our knowledge, only in Ref. 12. Zhang *et al.*[12] performed partial assignment: 11 out of 18 Raman-active modes predicted by factor-group analysis (FGA) within the $I4/m$ symmetry group. They found that only one mode around 180 $cm^{-1}$ exhibits a change in frequency around $T_c$. However, the origin of this mode remained unclear.

In this paper, RS is used to determine the influence of vacancy ordering on phonon spectra of $K_xFe_{2-y}Se_2$ single crystals. The polarized Raman spectra were analyzed in terms of peculiarities of both the $I4/m$ and $I4/mmm$ space group symmetries. Sixteen out of eighteen Raman-active phonons of the $I4/m$ and two Raman-active phonons of the $I4/mmm$ phase, predicted by FGA for our measurement configuration, have been observed and assigned. This confirms the existence of two crystallographic domains in our sample. High-resolution powder x-ray diffraction (PXRD) measurements on the same sample also indicate that the sample has coexisting $I4/m$ and $I4/mmm$ regions.

Single crystals of $K_xFe_{2-y}Se_2$ were grown and treated by the post-annealing and quenching technique described elsewhere in detail.[13,14] Before starting the RS measurements, the samples were cleaved in order to obtain a flat and shiny (001)-plane surface. The RS measurements were performed using a TriVista 557 Raman system in backscattering micro-Raman configuration. The 514.5 nm line of an $Ar^+/Kr^+$ mixed gas laser was used as an excitation source. The corresponding excitation power density was less than 0.2 $kW/cm^2$. All measurements were performed in the vacuum by using a KONTI CryoVac continuous helium flow cryostat with a 0.5 mm thick window.

PXRD measurements at room temperature and 400 °C were carried out at the X16C beamline of the National Synchrotron Light Source at Brookhaven National Laboratory. The measurements were made on the same sample, several months after preparation and the Raman experiments. The sample was sealed in a 1 mm diameter glass capillary with Si as an internal standard and dilutant, and diffraction data collected at a wavelength of 0.5612 Å from a channel-cut Si(111) monochromator and Ge(111) analyzer. PXRD results[15] were Rietveld refined with TOPAS Academic software;[16] see Fig. 1.

The sample's composition was previously measured by x-ray spectroscopy in an electron microscope to be $K_{0.64(4)}Fe_{1.44(4)}Se_2$.[17] A PXRD pattern at 400 °C refined to a single phase of composition $K_{0.72(4)}Fe_{1.60(4)}Se_2$. While the results of these two measurements differ by more than the stated uncertainty, we do not believe they are in disagreement due to possible systematic errors in both measurement techniques. The room-temperature data were analyzed as a mixture of two phases: an $I4/mmm$ phase structurally identical to the high-temperature structure, and the Fe vacancy-ordered $\sqrt{5} \times \sqrt{5}$ $I4/m$ phase. This two-phase description is in agreement with the recent STM study.[9] A fit to a single-phase model in $I4/m$ with partial vacancy ordering is significantly worse than the two-phase model ($\chi^2 = 2.88$ vs 2.28), and can therefore be excluded. The refined composition of the sample is $K_{0.68(2)}Fe_{1.57(3)}Se_2$, in satisfactory agreement with both the high-temperature PXRD and the x-ray spectroscopy results.

 

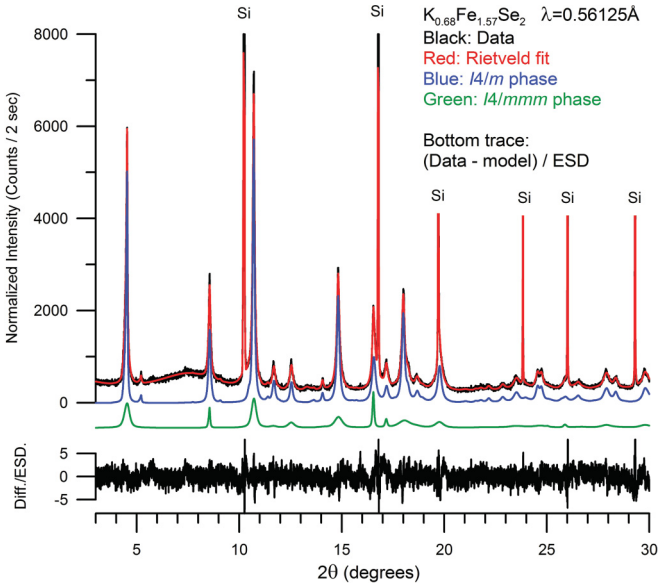


FIG. 1. (Color online) PXRD diffraction data with Rietveld fit, showing separate contributions from $I4/m$ and $I4/mmm$ phases. Peaks from the Si internal standard, in both the main plot and the scaled difference curve, are truncated. This fit has weighted $R$ factor $R_{WP} = 5.90\%$ and $\chi^2 = 2.28$.

Unit cells for both phases are built up of interspersed FeSe slabs and nets of K, stacked along the $z$ axis; see Fig. 2. Refined atomic positions and occupancies of both phases are listed in Table I. Note that the refined occupancy of the iron sites in the superconducting $I4/mmm$ phase is unity, within its standard uncertainty. On the other hand, neither Fe site in the $\sqrt{5} \times \sqrt{5}$ $I4/m$ phase is fully occupied.

One feature of note from the PXRD refinement (Fig. 1) is that the diffraction peaks of the $I4/mmm$ phase are substantially broader than those of the $I4/m$ phase. It is difficult to quantify the effect, because $I4/mmm$ peaks overlap the strongest $I4/m$ peaks and both phases exhibit significant anisotropic microstrain broadening; an estimate from the Scherrer equation leads to an $I4/mmm$ domain size on the order of 100 nm.

According to symmetry considerations one can expect four Raman-active phonons for the $I4/mmm$ phase and 27

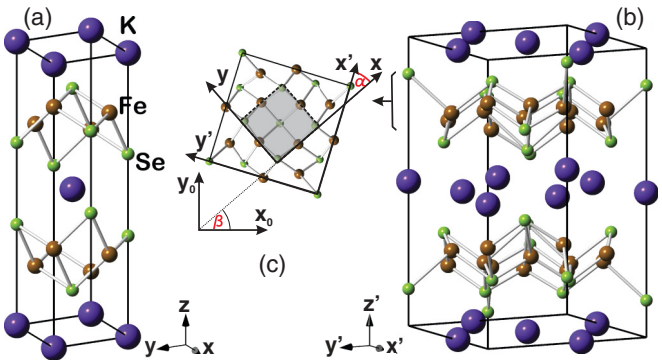


FIG. 2. (Color online) Crystal structure of $K_xFe_{2-y}Se_2$ in (a) $I4/mmm$ and (b) $I4/m$ unit cells (black lines). (c) FeSe slab in the (001) plane. The solid line illustrates the $I4/m$ unit cell and the shaded square illustrates the $I4/mmm$ unit cell.

TABLE I. Structural parameters for the $K_xFe_{2-y}Se_2$ two-phase powder sample at room temperature. Standard uncertainties given in parentheses are derived from counting statistics, and are generally smaller than plausible estimates of accuracy.

**Phase I**

Space group $I4/mmm$
Lattice $a = 3.898(1)$ Å, $c = 14.091(4)$ Å
Mole fraction 19(1)%

| Atom | Site | $x$ | $y$ | $z$ | Occ |
|---|---|---|---|---|---|
| K | 2*a* | 0 | 0 | 0 | 0.82(4) |
| Fe | 4*d* | 0 | 0.5 | 0.25 | 0.99(3) |
| Se | 4*e* | 0 | 0 | 0.354(1) | 1 |

**Phase II**

Space group $I4/m$
Lattice $a = 8.703(3)$ Å, $c = 14.160(1)$ Å
Mole fraction 81(1)%

| Atom | Site | $x$ | $y$ | $z$ | Occ |
|---|---|---|---|---|---|
| K1 | 2*b* | 0 | 0 | 0.5 | 1.00(6) |
| K2 | 8*h* | 0.583(4) | 0.242(2) | 0.5 | 0.56(2) |
| Fe1 | 16*i* | 0.296(1) | 0.596(1) | 0.247(1) | 0.84(1) |
| Fe2 | 4*d* | 0 | 0.5 | 0.25 | 0.33(2) |
| Se1 | 4*e* | 0 | 0 | 0.139(1) | 1 |
| Se2 | 16*i* | −0.089(1) | 0.302(1) | 0.353(1) | 1 |

Raman-active phonons for the $I4/m$ phase (Table II). When Raman scattering is measured at the (001) plane of the $K_xFe_{2-y}Se_2$ sample, two Raman-active phonons ($A_{1g} + B_{1g}$) of the $I4/mmm$ phase and 18 Raman-active phonons ($9A_g + 9B_g$) of the $I4/m$ phase can be observed. Here, one must have in mind that the $\mathbf{x}'$ and $\mathbf{y}'$ axes of the $I4/m$ phase are rotated by an angle $\alpha$ ($-\alpha$ for the twin domain),[18] to the corresponding axes ($\mathbf{x}$ and $\mathbf{y}$) of the $I4/mmm$ phase; see Fig. 2.

In general, the intensity of a given Raman-active phonon can be expressed as $I \sim |\boldsymbol{e}_s \hat{R} \boldsymbol{e}_i|^2$, where $\boldsymbol{e}_i$ and $\boldsymbol{e}_s$ are incident and scattered light polarization vectors.[19] $\hat{R}$ is Raman scattering tensor, a $3 \times 3$ complex matrix which describes the properties of the phonon with the respect to Raman scattering, expressed in the crystal principal axes basis. In order to obtain proper selection rules for $I4/mmm$ and $I4/m$ domains for the arbitrary crystal orientation (see Fig. 2), we have to transform the corresponding Raman tensors in terms of laboratory coordinate system $\mathbf{x}_0\mathbf{y}_0\mathbf{z}_0$, $\hat{R}^{x_0y_0z_0} = \Phi \hat{R}^{xyz} \tilde{\Phi}$. When measuring the Raman intensity of a phonon with polarization vectors $\boldsymbol{e}_s$ and $\boldsymbol{e}_i$ along the main axes of the Raman tensor, only the absolute value of one tensor component contributes to the Raman intensity. However, in other scattering geometries, where $\boldsymbol{e}_s$ and $\boldsymbol{e}_i$ are not parallel to the main axes of $\hat{R}$, the relative phase difference between Raman tensor elements influences the strength of the scattering process. For our scattering configuration in which $\boldsymbol{x_0} \parallel \boldsymbol{e}_s$ and $\Theta = \angle(\boldsymbol{e}_s, \boldsymbol{e}_i)$, the Raman intensities for the Raman tensors represented in Table II are given by

$$
\begin{aligned}
&I_{A_g}(\theta) \sim |a'|^2 \cos^2\theta, \quad I_{A_{1g}}(\theta) \sim |a|^2 \cos^2\theta, \\
&I_{B_g}(\theta) \sim (c' \cos[\theta + 2(\beta \pm \alpha)] + d' \sin[\theta + 2(\beta \pm \alpha)])^2, \\
&I_{B_{1g}}(\theta) \sim |c|^2 \cos^2(\theta + 2\beta). \qquad (1)
\end{aligned}
$$

Figure 3(a) displays $I(\theta)$ according to Eqs. (1) for one arbitrary choice of parameters with $\alpha = 27^\circ$ and $\beta = 50^\circ$. As can be

TABLE II. The type of atoms together with their site symmetries, each site's contributions to the Γ point phonons, as well as Raman tensors, phonon activities and selection rules for both $I4/mmm$ and $I4/m$ phases.

| $I4/mmm$ ($D_{4h}^{17}$ and $Z^B = 1$) | | $I4/m$ ($C_{4h}^{5}$ and $Z^B = 5$) | |
|---|---|---|---|
| Atoms (site symmetry) | Irreducible representations | Atoms (site symmetry) | Irreducible representations |
| K ($D_{4h}$) | $A_{2u} + E_u$ | K1 ($C_{4h}$) | $A_u + E_u$ |
| Fe ($D_{2d}$) | $A_{2u} + B_{1g} + E_g + E_u$ | K2 ($C_s$) | $2A_g + A_u + 2B_g + B_u + E_g + 2E_u$ |
| Se ($C_{4v}$) | $A_{1g} + A_{2u} + E_g + E_u$ | Fe1 ($C_1$) | $3A_g + 3A_u + 3B_g + 3B_u + 3E_g + 3E_u$ |
| | | Fe2 ($S_4$) | $A_u + B_g + E_g + E_u$ |
| | | Se1 ($C_4$) | $A_g + A_u + E_g + E_u$ |
| | | Se2 ($C_1$) | $3A_g + 3A_u + 3B_g + 3B_u + 3E_g + 3E_u$ |

Raman tensors

$$\hat{R}^{xyz}_{A_{1g}} = \begin{pmatrix} |a|e^{i\varphi_a} & 0 & 0 \\ 0 & |a|e^{i\varphi_a} & 0 \\ 0 & 0 & |b|e^{i\varphi_b} \end{pmatrix} \quad \hat{R}^{xyz}_{B_{1g}} = \begin{pmatrix} |c|e^{i\varphi_c} & 0 & 0 \\ 0 & -|c|e^{i\varphi_c} & 0 \\ 0 & 0 & 0 \end{pmatrix} \quad \hat{R}^{x'y'z}_{A_g} = \begin{pmatrix} |a'|e^{i\varphi'_a} & 0 & 0 \\ 0 & |a'|e^{i\varphi'_a} & 0 \\ 0 & 0 & |b'|e^{i\varphi'_b} \end{pmatrix} \quad \hat{R}^{x'y'z}_{B_g} = \begin{pmatrix} |c'|e^{i\varphi'_c} & |d'|e^{i\varphi'_d} & 0 \\ |d'|e^{i\varphi'_d} & -|c'|e^{i\varphi'_c} & 0 \\ 0 & 0 & 0 \end{pmatrix}$$

Activity and selection rules

$\Gamma_{\text{Raman}} = A_{1g}(\alpha_{xx+yy},\alpha_{zz}) + B_{1g}(\alpha_{xx-yy}) + 2E_g(\alpha_{xz},\alpha_{yz})$
$\Gamma_{\text{infrared}} = 2A_{2u}(\mathbf{E} \parallel \mathbf{z}) + 2E_u(\mathbf{E} \parallel \mathbf{x},\mathbf{E} \parallel \mathbf{y})$
$\Gamma_{\text{acoustic}} = A_u + E_u$

$\Gamma_{\text{Raman}} = 9A_g(\alpha_{x'x'+y'y'},\alpha_{zz}) + 9B_g(\alpha_{x'x'-y'y'},\alpha_{x'y'}) + 9E_g(\alpha_{x'z},\alpha_{y'z})$
$\Gamma_{\text{infrared}} = 9A_u(\mathbf{E} \parallel \mathbf{z}) + 7B_u(\text{silent}) + 10E_u(\mathbf{E} \parallel \mathbf{x}',\mathbf{E} \parallel \mathbf{y}')$
$\Gamma_{\text{acoustic}} = A_u + E_u$

seen, modes of the $B_g$ symmetry can be observed for every value of Θ, whereas the ones of the $A_g$ and $A_{1g}$ symmetry vanish for crossed polarization configuration, independently of the crystal orientation. The $B_{1g}$ reaches maximum intensity for $\Theta = -2\beta$ and vanishes for $\Theta = 90^\circ - 2\beta$.

Figure 3(b) shows RS spectra of $K_xFe_{2-y}Se_2$ single crystals measured at 85 and 270 K in parallel and crossed polarization configurations. First we will discuss the Raman modes of the high-symmetry phase $I4/mmm$. RS study of (Sr,K)$Fe_2As_2$,[20] isostructural to our high symmetry phase, revealed that the $A_{1g}$ and $B_{1g}$ symmetry modes appear at 185 and 210 $cm^{-1}$ (at 20 K). According to this assignment the peaks at about 180 and 207 $cm^{-1}$ (at 85 K, see Fig. 3) can be identified as the $A_{1g}$ and $B_{1g}$ symmetry vibrations of the As and Fe atoms of the high-symmetry phase, respectively. Appearance of the $B_{1g}$ mode at similar energies in both (Sr,K)$Fe_2As_2$ (210 $cm^{-1}$) and $K_xFe_{2-y}Se_2$ (207$cm^{-1}$) is expected since the lattice parameter $a$ for both crystal structures [(Sr,K)$Fe_2As_2$ and the $I4/mmm$ phase of $K_xFe_{2-y}Se_2$] are nearly the same and, as shown,[20] the substitution of K for Sr does not significantly change the frequencies of Raman modes involving As and Fe atom vibrations. Replacement of the lighter As atom with the heavier Se atom at the $C_{4v}$ site results only in a shift of the $A_{1g}$ mode in $K_xFe_{2-y}Se_2$ toward the lower energies (180 $cm^{-1}$), in comparison to the same mode in (Sr,K)$Fe_2As_2$ (185 $cm^{-1}$). The remarkable decrease of the $B_{1g}$ mode relative intensity with lowering temperature can be Fe vacancy order/disorder related.

Raman modes of the lower-symmetry phase ($I4/m$), Fig. 3(b), at 163 and 203 $cm^{-1}$ that are observed in parallel but not in crossed polarization configuration, are assigned as $A_g$ symmetry modes. Three modes at about 194, 188, and 214 $cm^{-1}$, which appear for the crossed polarization configuration, are assigned as $B_g$ modes.

Figure 4 shows Raman scattering spectra of $K_xFe_{2-y}Se_2$ single crystals measured at 85 K in four different polarization configurations. A multiple peak structure has been observed for parallel polarization configuration in the low-energy region between 80 and 150 $cm^{-1}$. By comparison of this spectral region with other polarization configurations (Fig. 4) we found that this structure consists of six Raman active modes, three of which (at about 107, 123, and 134 $cm^{-1}$) are of $A_g$ symmetry (blue lines in the inset of Fig. 4) and the remaining (at about

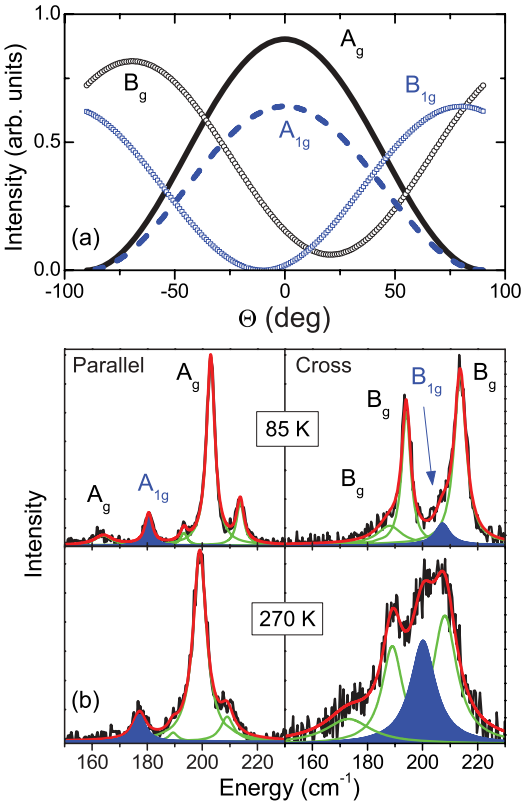


FIG. 3. (Color online) (a) Raman intensity angular dependencies of $A_g$, $B_g$, $A_{1g}$, and $B_{1g}$ modes for arbitrary parameters in the single-domain case. (b) Raman scattering spectra of $K_xFe_{2-y}Se_2$ single crystals measured in parallel and crossed polarization configurations. The sample was orientated so that $\boldsymbol{e_s} \parallel 1/\sqrt{2}[1,1,0]$ of the $I4/mmm$ phase.

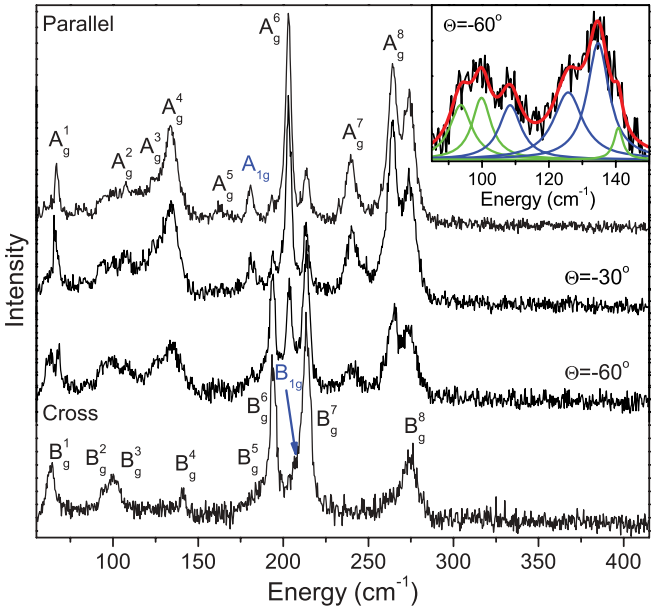


FIG. 4. (Color online) Raman scattering spectra of $K_xFe_{2-y}Se_2$ single crystals measured at 85 K in parallel ($\theta = 0°$), $\theta = 30°$, $\theta = 60°$, and cross ($\theta = 90°$) polarization configuration. Inset: Analysis of the $\theta = 60°$ spectra low-energy region using Lorentz lineshapes.

94, 100, and 140 cm$^{-1}$) are of $B_g$ symmetry (green lines in the inset of Fig. 4). The lowest-energy modes appear at 63 cm$^{-1}$ ($B_g$) and 67 cm$^{-1}$ ($A_g$). Analysis of the high-energy spectral region of the Raman spectra of $K_xFe_{2-y}Se_2$ single crystals (above 230 cm$^{-1}$) showed three peaks, which we assigned as $A_g$ symmetry modes (at about 240 and 264 cm$^{-1}$) and a $B_g$ symmetry one (274 cm$^{-1}$).

Figure 5(a) shows Raman scattering spectra of $K_xFe_{2-y}Se_2$ single crystals in the 160–225 cm$^{-1}$ spectral range measured at 85 K as a function of Θ. The relative intensities change of the analyzed modes as a function of Θ are presented in Fig. 5(b). The solid lines represent calculated spectra by using Eqs. (1) with one consistent set of parameters with the angle $\beta = 47(5)°$, which confirms the supposed orientation of the sample (see the caption of Fig. 3). When analyzing the $B_g$ mode relative intensity angular dependence, one must have in mind that $I4/m$ domains with the orientation $\alpha$ and $-\alpha$ appear with the same probability in the sample and both contribution must be taken into account. Analysis of the $A_{1g}$ and $B_{1g}$ modes' relative intensity angular dependences [Fig. 5(b)] also confirmed our previous assignment about the two-phase nature of the $K_xFe_{2-y}Se_2$ sample. Analysis of the 194 and 214 cm$^{-1}$ modes' relative intensities (denoted as $B_g^6$ and $B_g^7$) confirmed the $B_g$ nature of these modes. Additionally, we found that the angle between principal axes of the $I4/mmm$ and $I4/m$ phase domains in the (001) plane is about $\alpha = 29(6)°$, which is in agreement with the expected value of $\sim 26.6°$ for the $\sqrt{5} \times \sqrt{5}$ modulation.

In conclusion, Raman scattering was used to determine the influence of vacancy ordering on phonon spectra of $K_xFe_{2-y}Se_2$ single crystals. Polarized Raman spectra were analyzed in terms of peculiarities of both $I4/m$ and $I4/mmm$ symmetries. We have observed (at 85 K) $8A_g$ (67, 107, 123,

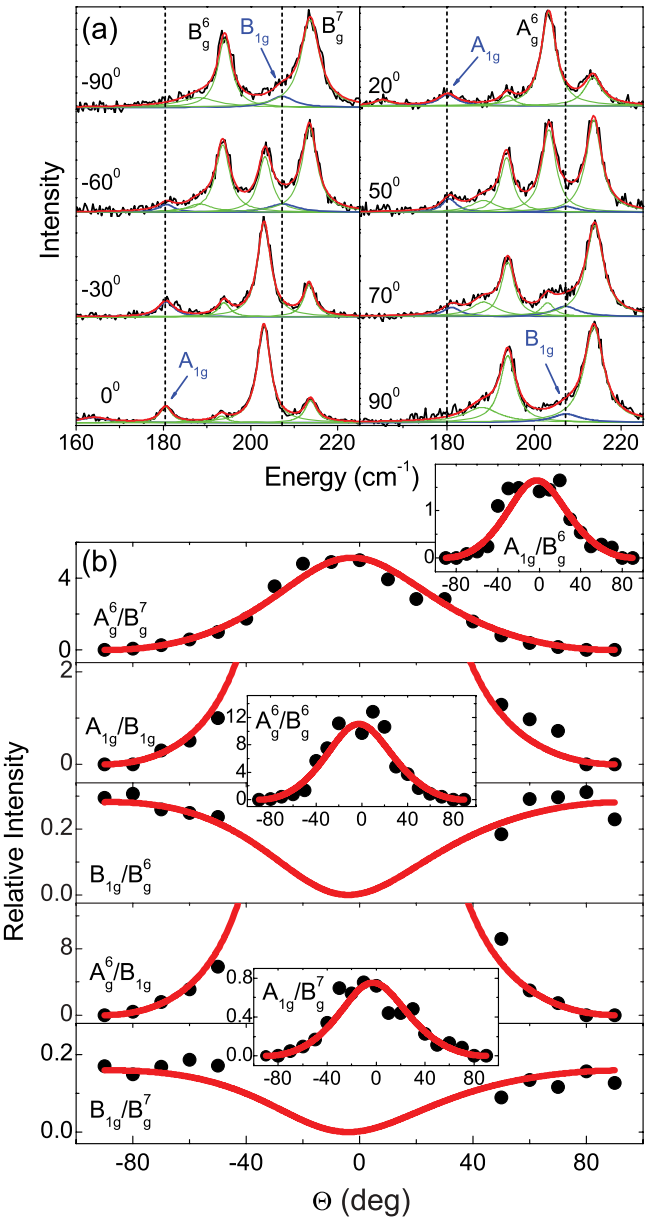


FIG. 5. (Color online) (a) Raman scattering spectra of $K_xFe_{2-y}Se_2$ single crystals measured at 85 K as a function of Θ. (b) Relative intensities of the Raman active modes as a function of Θ.

134, 163, 203, 240, and 264 cm$^{-1}$) and $8B_g$(63, 94, 100, 140, 188, 194, 214, and 274 cm$^{-1}$) modes originating from the vibrations of the $I4/m$ phase and $A_{1g}$ (180 cm$^{-1}$) and $B_{1g}$ (207 cm$^{-1}$) modes originating from the vibrations of the $I4/mmm$ phase. This confirmed the two-phase nature of $K_xFe_{2-y}Se_2$ sample. The structural refinement of the PXRD data of $K_xFe_{2-y}Se_2$ crystals confirmed the two-phase nature of the sample, as well as the fact that the Fe sites in the high-symmetry superconducting $I4/mmm$ phase are fully occupied, whereas there is a substantial density of Fe vacancies in the $\sqrt{5} \times \sqrt{5}$ $I4/m$ phase.

This work was supported by the Serbian Ministry of Education and Science under Projects No. ON171032 and

No. III45018. Work at Brookhaven is supported by the US Department of Energy (DOE) under Contract No. DE-AC02-98CH10886 (M.A. and E.S.B.) and in part by the Center for Emergent Superconductivity, an Energy Frontier Research Center funded by the DOE Office for Basic Energy Science (H.L. and C.P.).

[1]B. Wei, H. Qing-Zhen, C. Gen-Fu, M. A. Green, W. Du-Ming, H. Jun-Bao, and Q. Yi-Ming, Chin. Phys. Lett. **28**, 086104 (2011).

[2]G. M. Zhang, Z. Y. Lu, and T. Xiang, Phys. Rev. B **84**, 052502 (2011).

[3]F. Ye, S. Chi, W. Bao, X. F. Wang, J. J. Ying, X. H. Chen, H. D. Wang, C. H. Dong, and M. Fang, Phys. Rev. Lett. **107**, 137003 (2011).

[4]D. H. Ryan, W. N. Rowan-Weetaluktuk, J. M. Cadogan, R. Hu, W. E. Straszheim, S. L. Bud'ko, and P. C. Canfield, Phys. Rev. B **83**, 104526 (2011).

[5]V. Y. Pomjakushin, E. V. Pomjakushina, A. Krzton-Maziopa, K. Conder, and Z. Shermadini, J. Phys.: Condens. Matter **23**, 156003 (2011).

[6]Z. Shermadini, A. Krzton-Maziopa, M. Bendele, R. Khasanov, H. Luetkens, K. Conder, E. Pomjakushina, S. Weyeneth, V. Pomjakushin, O. Bossen, and A. Amato, Phys. Rev. Lett. **106**, 117602 (2011).

[7]P. Zavalij, W. Bao, X. F. Wang, J. J. Ying, X. H. Chen, D. M. Wang, J. B. He, X. Q. Wang, G. F. Chen, P.-Y. Hsieh, Q. Huang, and M. A. Green, Phys. Rev. B **83**, 132509 (2011).

[8]D. M. Wang, J. B. He, T.-L. Xia, and G. F. Chen, Phys. Rev. B **83**, 132502 (2011).

[9]W. Li, H. Ding, P. Deng, K. Chang, C. Song, K. He, L. Wang, X. Ma, J.-P. Hu, X. Chen, and Q.-K. Xue, Nat. Phys. **8**, 126 (2012).

[10]R. H. Yuan, T. Dong, Y. J. Song, P. Zheng, G. F. Chen, J. P. Hu, J. Q. Li, and N. L. Wang, Sci. Rep. **2**, 221 (2012).

[11]F. Chen, M. Xu, Q. Q. Ge, Y. Zhang, Z. R. Ye, L. X. Yang, Juan Jiang, B. P. Xie, R. C. Che, M. Zhang, A. F. Wang, X. H. Chen, D. W. Shen, J. P. Hu, and D. L. Feng, Phys. Rev. X **1**, 021020 (2011).

[12]A. M. Zhang, K. Liu, J. H. Xiao, J. B. He, D. M. Wang, G. F. Chen, B. Normand, and Q. M. Zhang, Phys. Rev. B **85**, 024518 (2012).

[13]F. Han, B. Shen, Z.-Y. Wang, and H.-H. Wen, arXiv:1103.1347.

[14]H. Lei and C. Petrovic, Phys. Rev. B **84**, 212502 (2011).

[15]See Supplemental Material at http://link.aps.org/supplemental/10.1103/PhysRevB.86.054503 for details of the powder crystal structure analysis.

[16]A. A. Coelho, TOPAS Academic v4.1 technical reference, www.topas-academic.net

[17]H. Lei, M. Abeykoon, E. S. Bozin, K. Wang, J. B. Warren, and C. Petrovic, Phys. Rev. Lett. **107**, 137002 (2011).

[18]V. Y. Pomjakushin, D. V. Sheptyakov, E. V. Pomjakushina, A. Krzton-Maziopa, K. Conder, D. Chernyshov, V. Svitlyk, and Z. Shermadini, Phys. Rev. B **83**, 144410 (2011).

[19]R. Loudon, Adv. Phys. **13**, 423 (1964).

[20]A. P. Litvinchuk, V. G. Hadjiev, M. N. Iliev, B. Lv, A. M. Guloy, and C. W. Chu, Phys. Rev. B **78**, 060503 (2008).